Orientation-Dependent Propulsion of Active Brownian Spheres: From Self-Advection to Programmable Cluster Shapes

Stephan Bröker,[1] Jens Bickmann,[1] Michael te Vrugt,[1] Michael E. Cates,[2] and Raphael Wittkowski[1,*]
[1]Institut für Theoretische Physik, Center for Soft Nanoscience, Westfälische Wilhelms-Universität Münster, 48149 Münster, Germany
[2]DAMTP, Centre for Mathematical Sciences, University of Cambridge, Cambridge CB3 0WA, United Kingdom

(Received 24 October 2022; accepted 25 August 2023; published 19 October 2023)

Applications of active particles require a method for controlling their dynamics. While this is typically achieved via direct interventions, indirect interventions based, e.g., on an orientation-dependent self-propulsion speed of the particles, become increasingly popular. In this Letter, we investigate systems of interacting active Brownian spheres in two spatial dimensions with orientation-dependent propulsion using analytical modeling and Brownian dynamics simulations. It is found that the orientation dependence leads to self-advection, circulating currents, and programmable cluster shapes.

DOI: 10.1103/PhysRevLett.131.168203

Active Brownian particles (ABPs) [1–4] combine Brownian motion with directed self-propulsion, leading to an inherently nonequilibrium dynamics. They are a prime model system for active particles, which have great potential for future applications including nanobots for medical applications like microsurgery [5] or drug delivery [6–8] and programmable materials for industrial applications [9–11]. Almost all applications have in common that general features of the dynamics of active particles, such as their collective dynamics, have to be controlled. This is often achieved using direct interventions [4,12], where an external force or torque acts on the particles. Recently, methods based on indirect interventions, where one instead changes the way the particles perceive their environment, have become very popular. Previous work on such approaches focuses on motility maps, where the particles' propulsion speed becomes space dependent [13–26]. Such systems have already been realized, e.g., via light-propelled particles in complex light fields [14,27]. Less well understood are indirect interventions with respect to the particles' orientations, as given, e.g., by an orientation-dependent propulsion force. Such forces arise, e.g., when particles are propelled by ultrasound [28] or light [29].

There exists theoretical as well as experimental work on single particles with an orientation-dependent self-propulsion [30,31], but many-particle systems of interacting ABPs with an orientation-dependent propulsion have not been investigated so far. Of particular importance in this context are the effects of such an indirect intervention on the collective dynamics of ABPs and their intriguing nonequilibrium effects, such as non-state-function pressure [32,33], reversed Ostwald ripening [34], and motility-induced phase separation (MIPS) [35].

In this Letter, we address this issue by investigating systems of interacting spherical ABPs with an orientation-dependent propulsion velocity in two spatial dimensions using analytical modeling and computer simulations. We derive a predictive field-theoretical model that describes the collective dynamics of such systems and find novel contributions that depend on the symmetry properties of the orientation-dependent propulsion. The model provides an analytical prediction for the spinodal corresponding to the onset of MIPS, which we compare to state diagrams obtained by Brownian dynamics simulations. Furthermore, we show that the orientation dependence of the propulsion gives rise to the self-assembly of deformed MIPS clusters with, e.g., elliptical, triangular, and rectangular shapes.

The considered system consists of N spherical, interacting ABPs in two spatial dimensions with center-of-mass positions $\boldsymbol{r}_i = (x_i, y_i)^{\mathrm{T}}$, orientations $\hat{\boldsymbol{u}}(\phi_i) = (\cos(\phi_i), \sin(\phi_i))^{\mathrm{T}}$, and polar orientation angles ϕ_i, where $i = 1, \ldots, N$. To model the microscopic dynamics of the particles, we use the Langevin equations

$$\dot{\boldsymbol{r}}_i = v_{\mathrm{A}}(\phi_i)\hat{\boldsymbol{u}}(\phi_i) + \boldsymbol{v}_{\mathrm{int},i}(\{\boldsymbol{r}_i\}) + \sqrt{2D_{\mathrm{T}}}\boldsymbol{\Lambda}_{\mathrm{T},i}, \quad (1)$$

$$\dot{\phi}_i = \sqrt{2D_{\mathrm{R}}}\Lambda_{\mathrm{R},i}, \quad (2)$$

where an overdot denotes a derivative with respect to time t. Equations (1) and (2) are overdamped (no momentum conservation). They differ from the standard Langevin equations for ABPs [2,3,12,33,36,37] by the orientation dependence of the propulsion speed $v_{\mathrm{A}}(\phi)$. Particle interactions are incorporated using the term $\boldsymbol{v}_{\mathrm{int},i}(\{\boldsymbol{r}_i\}) = -\beta D_{\mathrm{T}} \sum_{j=1, j\neq i}^{N} \boldsymbol{\nabla}_{\boldsymbol{r}_i} U_2(\|\boldsymbol{r}_i - \boldsymbol{r}_j\|)$. Here, $\beta = 1/(k_{\mathrm{B}}T)$ is the thermodynamic beta with Boltzmann constant k_{B} and temperature T, D_{T} the translational diffusion coefficient, $\boldsymbol{\nabla}_{\boldsymbol{r}_i} = (\partial_{x_i}, \partial_{y_i})^{\mathrm{T}}$ the del operator with respect to $\boldsymbol{r}_i$, U_2 a two-particle interaction potential, $\|\cdot\|$ the Euclidean norm, $D_{\mathrm{R}} = 3D_{\mathrm{T}}/a^2$ the rotational diffusion coefficient, and a the

particle diameter. Thermal fluctuations are modeled via zero-mean, unit-variance statistical white noises $\mathbf{\Lambda}_{\mathrm{T},i}(t)$ and $\Lambda_{\mathrm{R},i}(t)$.

Using the interaction-expansion method [36–41], we derived from Eqs. (1) and (2) an advection-diffusion model that describes the time evolution of the number density $\rho(\boldsymbol{r},t)$ of the particles, depending on position $\boldsymbol{r}=(x,y)^{\mathrm{T}}$ and time. The derivation (see the Supplemental Material [42]) assumes short-ranged interactions and a dependence of $v_{\mathrm{A}}(\phi)$ on ϕ that can be well approximated with few Fourier modes. The resulting model reads as

$$\dot{\rho}=-\boldsymbol{\nabla}\cdot(\boldsymbol{\mu}^{(1)}\rho)+\boldsymbol{\nabla}\cdot(\underline{D}(\rho)\boldsymbol{\nabla}\rho), \tag{3}$$

where $\underline{D}(\rho)$ is a density-dependent diffusion tensor with elements

$$D_{ij}(\rho)=(D_{\mathrm{T}}+c_1\rho+c_2\rho^2)\delta_{ij}+c_3\rho\mu_{ij}^{(2)}+\frac{\mu_{ik}^{(2)}\mu_{kj}^{(2)}}{2D_{\mathrm{R}}}. \tag{4}$$

(We sum over repeated lower indices from here on.) The coefficients c_i are given in the Supplemental Material [42]. Moreover, δ_{ij} denotes the Kronecker delta, $\boldsymbol{\mu}^{(1)}=\int_0^{2\pi}d\phi v_{\mathrm{A}}(\phi)\hat{\boldsymbol{u}}(\phi)/(2\pi)$ the particles' orientation-averaged propulsion velocity, and $\mu_{ij}^{(2)}$ the elements of the symmetric velocity tensor $\underline{\mu}^{(2)}=\int_0^{2\pi}d\phi v_{\mathrm{A}}(\phi)\hat{\boldsymbol{u}}(\phi)\otimes\hat{\boldsymbol{u}}(\phi)/\pi$ with the dyadic product $\otimes$. Formally, $\boldsymbol{\mu}^{(1)}$ and $\underline{\mu}^{(2)}$ are the zeroth- and first-order contributions, respectively, of the orientational expansion of the propulsion velocity $\boldsymbol{v}(\phi)=v_{\mathrm{A}}(\phi)\hat{\boldsymbol{u}}(\phi)$ into Cartesian tensors [47,48]: $\boldsymbol{v}(\phi)=\boldsymbol{\mu}^{(1)}+\hat{\boldsymbol{u}}(\phi)\cdot\underline{\mu}^{(2)}+\mathcal{O}(\hat{\boldsymbol{u}}^2)$. Including the $\mathcal{O}(\hat{\boldsymbol{u}}^2)$ contributions would not lead to additional terms in Eq. (3) unless we also include higher orders in derivatives. For the special case of an isotropic propulsion speed, we recover the purely diffusive model from Ref. [36]. In this case (i.e., $v_{\mathrm{A}}=\bar{v}$ with a constant $\bar{v}$), we get $\boldsymbol{\mu}^{(1)}=\boldsymbol{0}$ and $\mu_{ij}^{(2)}=\bar{v}\delta_{ij}$ such that $\boldsymbol{v}(\phi)=\bar{v}\,\hat{\boldsymbol{u}}(\phi)$ as required. Equation (3) is our first main result.

The orientational contributions $\boldsymbol{\mu}^{(1)}$ and $\underline{\mu}^{(2)}$ are the novel features of this model compared with the model derived in Ref. [36] for isotropic propulsion. A nonvanishing $\boldsymbol{\mu}^{(1)}$ corresponds to an internal polarization of the propulsion velocity that, similar to an external field [12], gives rise to (self-)advection. This is easily seen from the fact that the first term on the right-hand side of Eq. (3) can be eliminated using the Galilei transformation $\boldsymbol{r}\to\boldsymbol{r}-\boldsymbol{\mu}^{(1)}t$. The self-advection results, like the motility of individual active particles [49–51], from an $(\boldsymbol{r}\leftrightarrow-\boldsymbol{r})$-symmetry breaking. In contrast, $\underline{\mu}^{(2)}$ breaks the $(x\leftrightarrow y)$ symmetry of the diffusion tensor (4). This also occurs in systems with chirality such as circle swimmer systems [37,52].

For what follows, we specify the orientation-dependent propulsion speed $v_{\mathrm{A}}(\phi)$ as

$$v_{\mathrm{A},n}(\phi)=\bar{v}\big(1-\nu+2\nu\sin^2(n\phi/2)\big), \tag{5}$$

which involves an n-fold symmetry and is parametrized by the orientation-averaged propulsion speed $\bar{v}$ and the dimensionless angular modulation amplitude ν. In Ref. [31], active magnetic dumbbells with an orientation-dependent propulsion speed similar to (5) were realized experimentally. Therefore, the phenomena predicted in this Letter can be observed experimentally in systems of such dumbbells (and presumably also in many other systems). As was the case in the experiments from Ref. [31] (and as is common in active matter physics), the self-propulsion is implemented on the single-particle level. What we are interested in is the many-particle behavior resulting from Eq. (5).

We focus on the cases $n=1,\ldots,4$. Using Eq. (5), we obtain

$$\boldsymbol{\mu}^{(1)}=-\bar{v}\delta_{n,1}\frac{1}{2}(\nu,0)^{\mathrm{T}}, \tag{6}$$

$$\underline{\mu}^{(2)}=\bar{v}\left(\mathbb{1}-\underline{\sigma}_3\delta_{n,2}\frac{\nu}{2}\right), \tag{7}$$

where $\mathbb{1}$ is the identity matrix and $\underline{\sigma}_3$ is the third Pauli matrix. Physically, this result means that for $n=1$ (the only case with nonzero $\boldsymbol{\mu}^{(1)}$) there is a constant mean force in the x direction with an amplitude proportional to ν. For $n=2$, $\mu_{11}^{(2)}$ is decreased and $\mu_{22}^{(2)}$ increased, implying that the diffusivity is different for the x and y direction.

To investigate the system further, we performed Brownian dynamics simulations [53] based on the Langevin equations (1) and (2). For the interactions, we chose the Weeks-Chandler-Andersen potential $U_2(r)=(4\varepsilon[(a/r)^{12}-(a/r)^6]+\varepsilon)\Theta(2^{1/6}a-r)$ [54] with interaction strength ε, particle distance r, and Heaviside step function Θ. The particle diameter a, Lennard-Jones timescale $\tau_{\mathrm{LJ}}=a^2/(\varepsilon\beta D_{\mathrm{T}})$, and interaction strength ε are chosen as units of length, time, and energy, respectively. Nondimensionalization of Eqs. (1) and (2) leads to the Péclet number $\mathrm{Pe}=\bar{v}a/D_{\mathrm{T}}$, which is a measure for the activity of the particles, and the overall packing density $\Phi_0=\pi\bar{\rho}a^2/4$, where $\bar{\rho}$ is the spatially averaged number density of the particles. We fixed the average propulsion speed to $\bar{v}=24a/\tau_{\mathrm{LJ}}$ and changed Pe via the temperature T. If not stated otherwise, we chose $\mathrm{Pe}=150$ and $\Phi_0=0.4$. Additional details on the computer simulations can be found in the Supplemental Material [42].

Equation (6) predicts the self-advection velocity $\boldsymbol{\mu}^{(1)}$ of MIPS clusters for $n=1$. We confirmed this by comparing Eq. (6) with the velocity $\boldsymbol{v}_{\mathrm{c}}=(v_{\mathrm{c},x},v_{\mathrm{c},y})^{\mathrm{T}}$ of macroscopic MIPS clusters of ABPs that we observed in Brownian dynamics simulations. Figure 1 shows that our analytical prediction and the velocity of the clusters are in excellent agreement, demonstrating that our theory is applicable also to self-organized structures. The x component of $\boldsymbol{v}_{\mathrm{c}}$

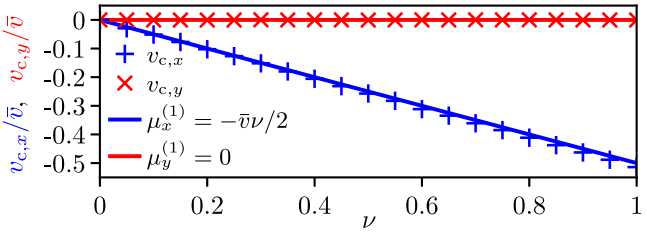

FIG. 1. Comparison of our analytical results for the self-advection velocity $\boldsymbol{\mu}^{(1)} = (\mu_x^{(1)}, \mu_y^{(1)})^{\mathrm{T}}$ [see Eq. (6)] with the time-averaged velocity of particle clusters $\boldsymbol{v}_{\mathrm{c}} = (v_{\mathrm{c},x}, v_{\mathrm{c},y})^{\mathrm{T}}$ that we obtained from six Brownian dynamics simulations for each considered value of the angular modulation amplitude ν.

decreases linearly for increasing ν, and the y component is zero since $v_{\mathrm{A},1}(\phi) = v_{\mathrm{A},1}(-\phi)$. Our results suggest that, by changing the first Fourier mode of $v_{\mathrm{A}}(\phi)$, one can steer many-particle structures of ABPs in arbitrary directions. This effect can be useful for applications where one wants, e.g., to steer clusters of ABPs through a maze or into or out of a trap, including active carrier particles that need to swim to certain regions and release their cargo there [6–8]. The ability to steer ABPs collectively is relevant, e.g., for drug delivery [55] and active microstructures [15].

For $n = 2$, no self-advection arises, but the diffusion tensor has no longer identical diagonal elements: $D_{ij} \propto f(\rho)\delta_{ij} - \bar{v}\nu(c_3\rho + \bar{v}/D_{\mathrm{R}})\sigma_{3,ij}$ with a scalar function $f(\rho)$. Since the diffusion tensor determines the spinodal for the onset of MIPS [36], the spinodal differs from the standard case. A linear stability analysis yields the spinodal condition $D_{22}(\rho) = 0$. This condition becomes equal to the one presented in Ref. [36] for standard ABPs with isotropic propulsion when one replaces the ordinary Péclet number there by a new effective Péclet number $\mathrm{Pe}_{\mathrm{eff}} = a\max(\mu_{11}^{(2)}, \mu_{22}^{(2)})/D_{\mathrm{T}} = (1 + \nu/2)\mathrm{Pe}$. To confirm the spinodal condition and this mapping, we obtained, for different angular modulation amplitudes ν, state diagrams by Brownian dynamics simulations. We chose the standard deviation of the reduced interaction energy $\sigma(E_{\mathrm{int}}/\varepsilon)$ [37] as a quantity for the identification of clusters. The analytical prediction and simulation results for the spinodal are shown in Fig. 2.

For $\nu = 0$, which corresponds to standard MIPS, the state diagram [see Fig. 2(a)] shows a homogeneous state for low Φ_0, a solid state for small Pe and large Φ_0, and MIPS clusters for large Pe and moderate or large Φ_0. Both of the latter two states have a higher standard deviation of the reduced interaction energy $\sigma(E_{\mathrm{int}}/\varepsilon)$ than the homogeneous state. For increasing ν, the state diagram gradually changes and the MIPS clusters emerge at lower Pe [see Figs. 2(b) and 2(c)]. The analytical prediction exhibits the same qualitative behavior and is in very good agreement with the simulation data even for large modulation amplitudes $\nu = 1$. As shown in Fig. 2(d), while the value Pe_{c} of Pe at the critical point decreases with ν, the critical value $\mathrm{Pe}_{\mathrm{eff,c}}$ of $\mathrm{Pe}_{\mathrm{eff}}$ remains (like the critical value $\Phi_{0,\mathrm{c}}$ of Φ_0) unchanged. In addition, we determined the critical point directly from the simulations via the improved finite-size scaling method developed in Ref. [56] (see the Supplemental Material [42] for details). The results, which are plotted in Fig. 2(d), are in good agreement with the theoretical prediction. This confirms our claim that one can map the phase-separation behavior onto that of standard ABPs by making use of an effective Péclet number. What is not captured by the analytical prediction is the fact that the spinodal is numerically found to move upward for larger ν. This effect can be understood by noting that for larger ν, the particles are fast for $\phi \approx 0, \pi$ and slow for $\phi \approx \pi/2, 3\pi/2$, and can therefore be thought of as a mixture of active and passive particles. For such mixtures, it has been found that the spinodal is shifted upward in the $\mathrm{Pe} - \Phi_0$ diagram compared with the purely active case [38]. The spinodal for MIPS is our second main result.

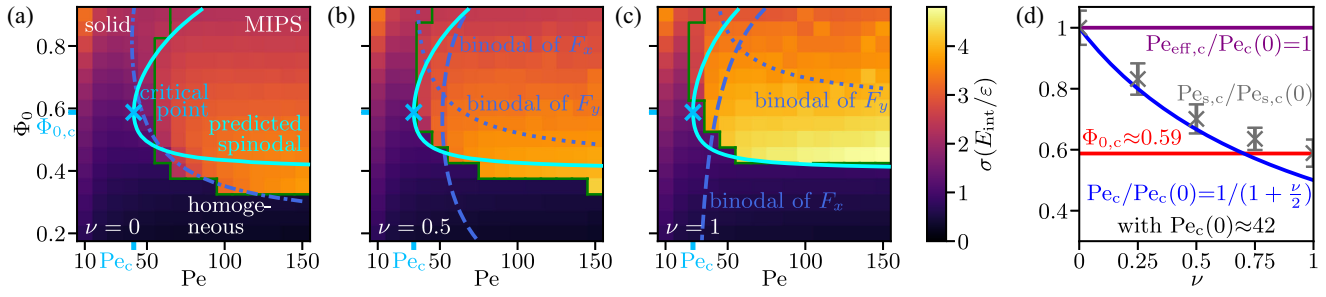

FIG. 2. (a)–(c) State diagrams for ABPs with orientation-dependent propulsion speed $v_{\mathrm{A},2}(\phi)$ [see Eq. (5)] showing the standard deviation of the reduced interaction energy $\sigma(E_{\mathrm{int}}/\varepsilon)$ as a function of the particles' Péclet number Pe and overall packing density Φ_0 for different values of the angular modulation amplitude ν. The state diagrams include a homogeneous state, MIPS, and a solid state. The green line is a guide to the eye of the border between MIPS and homogeneous distribution. Our analytical prediction for the spinodal corresponding to the onset of MIPS, the binodals estimated from F_x and F_y, and the critical point are indicated by light blue curves, dark blue curves, and light blue cross marks, respectively. (d) Predicted values of Pe, $\mathrm{Pe}_{\mathrm{eff}}$, and Φ_0 at the critical point (denoted Pe_{c}, $\mathrm{Pe}_{\mathrm{eff,c}}$, and $\Phi_{0,\mathrm{c}}$) and critical Péclet number obtained from the simulations (denoted $\mathrm{Pe}_{\mathrm{s,c}}$ and indicated by gray crosses with error bars) as a function of ν.

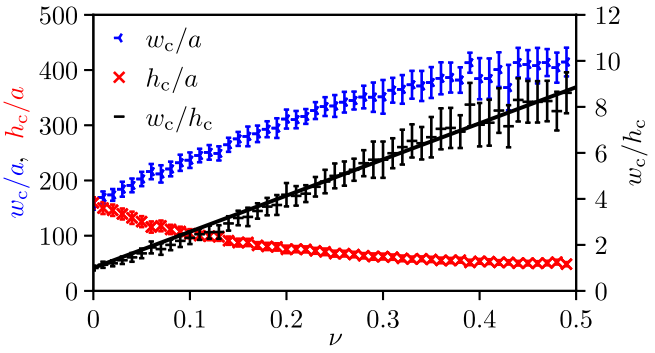

FIG. 3. Width w_c, height h_c, and aspect ratio w_c/h_c of MIPS clusters consisting of ABPs with propulsion speed $v_{A,2}(\phi)$ [see Eq. (5)] as functions of the angular modulation amplitude ν.

We also consider the binodal. For $\nu = 2$, Eq. (3) can be written as

$$\dot{\rho} = \partial_x\left(\rho\partial_x \frac{\delta F_x}{\delta\rho}\right) + \partial_y\left(\rho\partial_y \frac{\delta F_y}{\delta\rho}\right) \tag{8}$$

with free energies F_x and F_y (see the Supplemental Material [42]). For $F_x = F_y$, Eq. (8) would constitute an effective passive model and the binodal could be inferred from the free energy. In the present case, the orientation-dependent propulsion breaks this structure. We can nevertheless calculate the binodals for both F_x and F_y, which are plotted in Fig. 2. (Their relation to the actual binodal is discussed in the Supplemental Material [42].) Owing to strong approximations involved in their derivation (see the Supplemental Material [42]), the binodals are not quantitatively accurate (and not fully consistent with our accurate spinodal, which cannot lie outside the binodals in practice). Nevertheless, it is clear that they change as a function of v_A.

For $n = 2$, but not for $n = 1$, we also observed a deformation of MIPS clusters from (standard) circular [35] to elliptic shapes. This effect is captured in Fig. 3, where the width w_c, height h_c, and aspect ratio w_c/h_c of the clusters are shown. Interestingly, width and height change in such a way that the aspect ratio increases approximately linearly with ν, as shown by a linear fit in Fig. 3. This increase can be explained by the fact that, if $v_A(\phi)$ is given by Eq. (5) with $n = 2$, the difference between the magnitudes of the active forces from the y direction [proportional to $v_A(\pi/2)$] and x direction [proportional to $v_A(0)$] grows linearly with ν. A possible explanation for the elliptical shape is based on the fact that clusters in phase separation processes are usually spherical because this minimizes the total energy in a system of particles with attractive interactions. Such attractive interactions are present, on an effective level, in ABPs [57]. In the present case, the activity and therefore the attractive interactions are stronger for $\phi \approx \pi/2,\ 3\pi/2$ than for $\phi \approx 0, \pi$, implying that the system has a stronger tendency to minimize its surface curvature for $\phi \approx \pi/2,\ 3\pi/2$.

This leads to the question of whether one can use orientation-dependent propulsion speeds to induce clusters of arbitrary intended shapes in ABP systems. To follow this idea, we investigated also the cases $n = 3$ and $n = 4$, choosing $\nu = 0.25$ for $n = 2$ to avoid unreasonably large aspect ratios of the clusters and $\nu = 1$ otherwise to maximize the deformation phenomenon. The results are shown in Fig. 4. We observed elliptic clusters for $n = 2$ [see Fig. 4(a)], triangular clusters for $n = 3$ [see Fig. 4(b)], and rectangular clusters for $n = 4$ [see Fig. 4(c)]. The elliptic and triangular clusters occur so reliably that they are also clearly visible when averaging the particle distribution in the stationary state over 11 simulation runs and over time

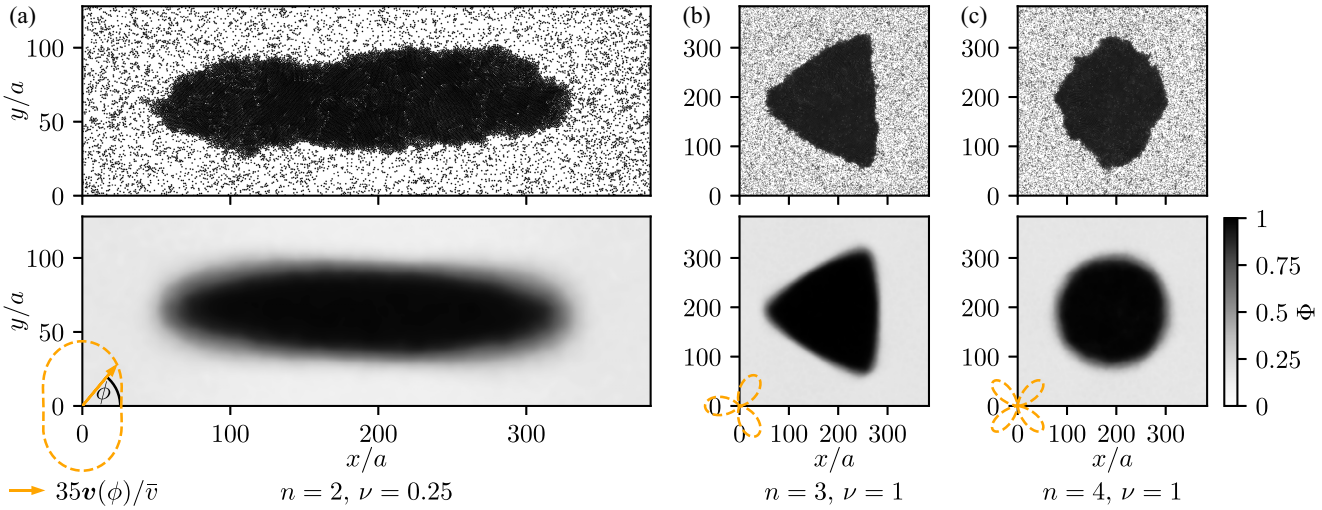

FIG. 4. Observed nonspherical cluster shapes that are self-assembled by ABPs with orientation-dependent propulsion speed $v_{A,n}(\phi)$ (see Eq. (5) for different values of the symmetry order n and angular modulation amplitude ν. Snapshots of particle-based simulations (top), performed by solving Eqs. (1), (2), and (5), and local packing densities $\Phi(x, y)$, obtained by averaging over these simulations and over time, (bottom) are shown for (**a**) elliptic, (**b**) triangular, and (**c**) rectangular clusters.

(bottom row of Fig. 4). In contrast, the rectangular clusters occur with their edges oriented either parallel to the coordinate axes or tilted by an angle $\pi/4$, such that this cluster shape is blurred by the averaging. The shape becomes rounder (and more like that of a system with isotropic propulsion) for larger n; see the Supplemental Material [42] for details. Clusters with more complex shapes can be realized by a more complex dependence of v_A on ϕ (and possibly $\boldsymbol{r}$).

These interesting findings may be utilized for the realization of programmable materials [15,58]. If the orientation-dependent propulsion can be controlled sufficiently well, the observed effect can make systems of active particles self-assemble into desired patterns. For example, electrically conducting ABPs may assemble switches where the elliptic clusters are used as bridges with certain orientations. The investigation of the programmable MIPS cluster shapes is our third main result.

Interestingly, the model (3) allows for circulating particle currents for $\underline{\mu}^{(2)} \neq \underline{0}$ since the curl of the current does not generally vanish in this case. Such currents are a central feature of active matter [59]. For $v_A = v_{A,2}$, Eq. (3) involves terms $\propto (\partial_x^2 - \partial_y^2)\rho^2$, which imply fluxes toward the denser region in the y direction and out of it in the x direction. This is related to the unusual MIPS cluster formation, since MIPS arises once particle fluxes point toward denser regions [60]. We therefore measured the current $\boldsymbol{J}(\boldsymbol{r})$ and the polarization $\boldsymbol{P}(\boldsymbol{r})$ (see the Supplemental Material [42] for definitions) in simulations for $n = 2$ to check whether circulating currents do in fact exist in the elliptic steady state. The results, which confirm this expectation, are shown in Fig. 5. Particles flow into the cluster from the y direction (large v_A) and out of it in the x direction (small v_A). This behavior is in stark contrast to the one known from standard ABPs, where there is no particle current through the interface in steady state [33,34]. Notably, $\boldsymbol{P}$ does always point inward at the boundary of the ellipse, such that $\boldsymbol{J}$ and $\boldsymbol{P}$ have opposite directions for $\phi \in \{0, \pi\}$ (see inset in Fig. 5). The particles on the left- and right-hand side are therefore pushed out of the cluster by interaction forces even though their self-propulsion force

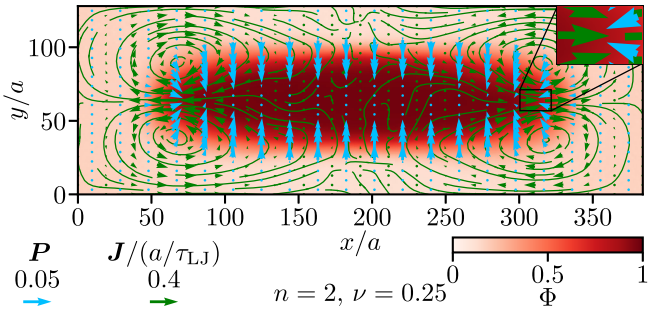

FIG. 5. Circulating currents in a stationary elliptic cluster for an orientation-dependent propulsion speed $v_{A,n}(\phi)$ with $n = 2$ and $\nu = 0.25$ [see Eq. (5)].

(parallel to $\boldsymbol{P}$) points toward the cluster. A video of the cluster formation and the resulting steady state (including circulating currents) can be found in Ref. [61]. The circulating currents are our fourth main result.

In summary, we have shown that the collective behavior of ABPs with orientation-dependent propulsion gives rise to fascinating effects including tunable self-advection and circulating particle currents. An effective Péclet number allows one to map the spinodal for the anomalous MIPS observed here onto that of standard MIPS. The orientation-dependent propulsion can be employed to induce self-assembly of nonspherical clusters. Our findings provide new insights into the intriguing nonequilibrium dynamics of active particles and constitute an important step toward the realization of programmable materials by active soft matter.

The supporting data for this Letter, including the raw data for all figures, are openly available from [61].

M. t. V. thanks the Studienstiftung des deutschen Volkes for financial support. M. E. C. is funded by the Royal Society. R. W. is funded by the Deutsche Forschungsgemeinschaft (DFG, German Research Foundation)—283183152 (WI 4170/3-2). The simulations for this work were performed on the computer cluster PALMA II of the University of Münster.

S. B. and J. B. contributed equally to this work.

*Corresponding author: raphael.wittkowski@uni-muenster.de

[1] J. Elgeti, R. G. Winkler, and G. Gompper, Physics of microswimmers—single particle motion and collective behavior: A review, Rep. Prog. Phys. **78**, 056601 (2015).
[2] T. Speck, Collective behavior of active Brownian particles: From microscopic clustering to macroscopic phase separation, Eur. Phys. J. Spec. Top. **225**, 2287 (2016).
[3] A. Zöttl and H. Stark, Emergent behavior in active colloids, J. Phys. Condens. Matter **28**, 253001 (2016).
[4] C. Bechinger, R. Di Leonardo, H. Löwen, C. Reichhardt, G. Volpe, and G. Volpe, Active particles in complex and crowded environments, Rev. Mod. Phys. **88**, 045006 (2016).
[5] T. Kurinomaru, A. Inagaki, M. Hoshi, C. Nakamura, and H. Yamazoe, Protein microswimmers capable of delivering cells for tissue engineering applications, Mater. Horiz. **7**, 877 (2020).
[6] Y. Alapan, O. Yasa, O. Schauer, J. Giltinan, A. F. Tabak, V. Sourjik, and M. Sitti, Soft erythrocyte-based bacterial microswimmers for cargo delivery, Sci. Rob. **3**, eaar4423 (2018).
[7] O. Yasa, P. Erkoc, Y. Alapan, and M. Sitti, Microalga-powered microswimmers toward active cargo delivery, Adv. Mater. **30**, 1804130 (2018).
[8] H. Ceylan, I. C. Yasa, O. Yasa, A. F. Tabak, J. Giltinan, and M. Sitti, 3D-printed biodegradable microswimmer for theranostic cargo delivery and release, ACS Nano **13**, 3353 (2019).

[9] S. Tibbits, 4D printing: Multi-material shape change, Archit. Des. **84**, 116 (2014).
[10] M. R. Jones, N. C. Seeman, and C. A. Mirkin, Programmable materials and the nature of the DNA bond, Science **347**, 1260901 (2015).
[11] S. Qi, H. Guo, J. Fu, Y. Xie, M. Zhu, and M. Yu, 3D printed shape-programmable magneto-active soft matter for biomimetic applications, Compos. Sci. Technol. **188**, 107973 (2020).
[12] J. Bickmann, S. Bröker, M. te Vrugt, and R. Wittkowski, Active Brownian particles in external force fields: Field-theoretical models, generalized barometric law, and programmable density patterns, Phys. Rev. E **108**, 044601 (2023).
[13] M. P. Magiera and L. Brendel, Trapping of interacting propelled colloidal particles in inhomogeneous media, Phys. Rev. E **92**, 012304 (2015).
[14] C. Lozano, B. ten Hagen, H. Löwen, and C. Bechinger, Phototaxis of synthetic microswimmers in optical landscapes, Nat. Commun. **7**, 12828 (2016).
[15] J. Stenhammar, R. Wittkowski, D. Marenduzzo, and M. E. Cates, Light-induced self-assembly of active rectification devices, Sci. Adv. **2**, e1501850 (2016).
[16] A. Geiseler, P. Hänggi, and F. Marchesoni, Self-polarizing microswimmers in active density waves, Sci. Rep. **7**, 41884 (2017).
[17] A. Sharma and J. M. Brader, Brownian systems with spatially inhomogeneous activity, Phys. Rev. E **96**, 032604 (2017).
[18] J. Grauer, H. Löwen, and L. M. C. Janssen, Spontaneous membrane formation and self-encapsulation of active rods in an inhomogeneous motility field, Phys. Rev. E **97**, 022608 (2018).
[19] B. Liebchen and H. Löwen, Optimal navigation strategies for active particles, Europhys. Lett. **127**, 34003 (2019).
[20] C. Lozano, B. Liebchen, B. ten Hagen, C. Bechinger, and H. Löwen, Propagating density spikes in light-powered motility-ratchets, Soft Matter **15**, 5185 (2019).
[21] C. Lozano and C. Bechinger, Diffusing wave paradox of phototactic particles in traveling light pulses, Nat. Commun. **10**, 2495 (2019).
[22] L. Caprini, U. Marini Bettolo Marconi, R. Wittmann, and H. Löwen, Dynamics of active particles with space-dependent swim velocity, Soft Matter **18**, 1412 (2022).
[23] L. Caprini, U. Marini Bettolo Marconi, R. Wittmann, and H. Löwen, Active particles driven by competing spatially dependent self-propulsion and external force, SciPost Phys. **13**, 065 (2022).
[24] J. Arlt, V. A. Martinez, A. Dawson, T. Pilizota, and W. C. K. Poon, Painting with light-powered bacteria, Nat. Commun. **9**, 768 (2018).
[25] G. Frangipane, D. Dell'Arciprete, S. Petracchini, C. Maggi, F. Saglimbeni, S. Bianchi, G. Vizsnyiczai, M. L. Bernardini, and R. Di Leonardo, Dynamic density shaping of photokinetic *E. coli*, eLife **7**, e36608 (2018).
[26] J. Arlt, V. A. Martinez, A. Dawson, T. Pilizota, and W. C. K. Poon, Dynamics-dependent density distribution in active suspensions, Nat. Commun. **10**, 2321 (2019).
[27] B. Dai, J. Wang, Z. Xiong, X. Zhan, W. Dai, C.-C. Li, S.-P. Feng, and J. Tang, Programmable artificial phototactic microswimmer, Nat. Nanotechnol. **11**, 1087 (2016).
[28] J. Voß and R. Wittkowski, Orientation-dependent propulsion of triangular nano- and microparticles by a traveling ultrasound wave, ACS Nano **16**, 3604 (2022).
[29] J. Jeggle, M. Rüschenbaum, C. Denz, and R. Wittkowski, Light-driven microswimmers with a symmetry breaking refractive index profile (to be published).
[30] W. E. Uspal, Theory of light-activated catalytic Janus particles, J. Chem. Phys. **150**, 114903 (2019).
[31] A. R. Sprenger, M. A. Fernandez-Rodriguez, L. Alvarez, L. Isa, R. Wittkowski, and H. Löwen, Active Brownian motion with orientation-dependent motility: Theory and experiments, Langmuir **36**, 7066 (2020).
[32] A. P. Solon, Y. Fily, A. Baskaran, M. E. Cates, Y. Kafri, M. Kardar, and J. Tailleur, Pressure is not a state function for generic active fluids, Nat. Phys. **11**, 673 (2015).
[33] A. P. Solon, J. Stenhammar, R. Wittkowski, M. Kardar, Y. Kafri, M. E. Cates, and J. Tailleur, Pressure and Phase Equilibria in Interacting Active Brownian Spheres, Phys. Rev. Lett. **114**, 198301 (2015).
[34] E. Tjhung, C. Nardini, and M. E. Cates, Cluster Phases and Bubbly Phase Separation in Active Fluids: Reversal of the Ostwald Process, Phys. Rev. X **8**, 031080 (2018).
[35] M. E. Cates and J. Tailleur, Motility-induced phase separation, Annu. Rev. Condens. Matter Phys. **6**, 219 (2015).
[36] J. Bickmann and R. Wittkowski, Predictive local field theory for interacting active Brownian spheres in two spatial dimensions, J. Phys. Condens. Matter **32**, 214001 (2020).
[37] J. Bickmann, S. Bröker, J. Jeggle, and R. Wittkowski, Analytical approach to chiral active systems: Suppressed phase separation of interacting Brownian circle swimmers, J. Chem. Phys. **156**, 194904 (2022).
[38] R. Wittkowski, J. Stenhammar, and M. E. Cates, Nonequilibrium dynamics of mixtures of active and passive colloidal particles, New J. Phys. **19**, 105003 (2017).
[39] J. Bickmann and R. Wittkowski, Collective dynamics of active Brownian particles in three spatial dimensions: A predictive field theory, Phys. Rev. Res. **2**, 033241 (2020).
[40] M. te Vrugt, T. Frohoff-Hülsmann, E. Heifetz, U. Thiele, and R. Wittkowski, From a microscopic inertial active matter model to the Schrödinger equation, Nat. Commun. **14**, 1302 (2023).
[41] M. te Vrugt, J. Bickmann, and R. Wittkowski, How to derive a predictive field theory for active Brownian particles: A step-by-step tutorial, J. Phys. Condens. Matter **35**, 313001 (2023).
[42] See Supplemental Material at http://link.aps.org/supplemental/10.1103/PhysRevLett.131.168203, which includes Refs. [43–46], for details on the derivation of Eq. (3) (Sec. I), the computer simulations (Sec. II), the calculation of the binodals (Sec. III), and the phase behavior (Sec. IV).
[43] J. Jeggle, J. Stenhammar, and R. Wittkowski, Pair-distribution function of active Brownian spheres in two spatial dimensions: Simulation results and analytic representation, J. Chem. Phys. **152**, 194903 (2020).
[44] A. J. M. Yang, P. D. Fleming, and J. H. Gibbs, Molecular theory of surface tension, J. Chem. Phys. **64**, 3732 (1976).

[45] M. E. Cates and J. Tailleur, When are active Brownian particles and run-and-tumble particles equivalent? Consequences for motility-induced phase separation, Europhys. Lett. **101**, 20010 (2013).
[46] Wolfram Research, Inc., Mathematica, Version 13.1, Champaign, IL, 2022, https://www.wolfram.com/mathematica.
[47] M. te Vrugt and R. Wittkowski, Relations between angular and Cartesian orientational expansions, AIP Adv. **10**, 035106 (2020).
[48] M. te Vrugt and R. Wittkowski, Orientational order parameters for arbitrary quantum systems, Ann. Phys. (Berlin) **532**, 2000266 (2020).
[49] A. Walther and A. H. E. Müller, Janus particles, Soft Matter **4**, 663 (2008).
[50] A. Walther and A. H. E. Müller, Janus particles: Synthesis, self-assembly, physical properties, and applications, Chem. Rev. **113**, 5194 (2013).
[51] J. Voß and R. Wittkowski, On the shape-dependent propulsion of nano- and microparticles by traveling ultrasound waves, Nanoscale Adv. **2**, 3890 (2020).
[52] G.-J. Liao and S. H. L. Klapp, Clustering and phase separation of circle swimmers dispersed in a monolayer, Soft Matter **14**, 7873 (2018).
[53] S. Plimpton, Fast parallel algorithms for short-range molecular dynamics, J. Comput. Phys. **117**, 1 (1995).
[54] J. D. Weeks, D. Chandler, and H. C. Andersen, Role of repulsive forces in determining the equilibrium structure of simple liquids, J. Chem. Phys. **54**, 5237 (1971).
[55] T. Nitschke, J. Stenhammar, and R. Wittkowski, Collective guiding of acoustically propelled nano- and microparticles, Nanoscale Adv. **4**, 2844 (2022).
[56] J. T. Siebert, F. Dittrich, F. Schmid, K. Binder, T. Speck, and P. Virnau, Critical behavior of active Brownian particles, Phys. Rev. E **98**, 030601(R) (2018).
[57] T. F. F. Farage, P. Krinninger, and J. M. Brader, Effective interactions in active Brownian suspensions, Phys. Rev. E **91**, 042310 (2015).
[58] J. Yan, M. Han, J. Zhang, C. Xu, E. Luijten, and S. Granick, Reconfiguring active particles by electrostatic imbalance, Nat. Mater. **15**, 1095 (2016).
[59] M. E. Cates, Active field theories, in *Active Matter and Nonequilibrium Statistical Physics, Lecture Notes of the Les Houches Summer School: Volume 112, 2018*, edited by J. Tailleur, G. Gompper, M. C. Marchetti, J. M. Yeomans, and C. Salomon (Oxford University Press, Oxford, 2022), pp. 180–216, 10.1093/oso/9780192858313.003.0006.
[60] J. Bialké, H. Löwen, and T. Speck, Microscopic theory for the phase separation of self-propelled repulsive disks, Europhys. Lett. **103**, 30008 (2013).
[61] S. Bröker, J. Bickmann, M. te Vrugt, M. E. Cates, and R. Wittkowski, Supplemental data for "Orientation-dependent propulsion of active Brownian spheres: from self-advection to programmable cluster shapes", Zenodo (2022), 10.5281/zenodo.6008487.